

Improving snow cover mapping in forests through the use of a canopy reflectance model

Andrew G. Klein,^{1,2,*} Dorothy K. Hall² and George A. Riggs,^{2,3}

¹*USRA, Seabrook, MD 20706, USA*

²*Hydrological Sciences Branch Mail Code 974, Laboratory for Hydrospheric Processes, NASA/Goddard Space Flight Center, Greenbelt, MD 20771, USA*

³*Research and Data Systems Corporation, Greenbelt, MD 20770, USA*

Abstract:

MODIS, the moderate resolution imaging spectroradiometer, will be launched in 1998 as part of the first earth observing system (EOS) platform. Global maps of land surface properties, including snow cover, will be created from MODIS imagery. The MODIS snow-cover mapping algorithm that will be used to produce daily maps of global snow cover extent at 500 m resolution is currently under development. With the exception of cloud cover, the largest limitation to producing a global daily snow cover product using MODIS is the presence of a forest canopy.

A Landsat Thematic Mapper (TM) time-series of the southern Boreal Ecosystem–Atmosphere Study (BOREAS) study area in Prince Albert National Park, Saskatchewan, was used to evaluate the performance of the current MODIS snow-cover mapping algorithm in varying forest types. A snow reflectance model was used in conjunction with a canopy reflectance model (GeoSAIL) to model the reflectance of a snow-covered forest stand. Using these coupled models, the effects of varying forest type, canopy density, snow grain size and solar illumination geometry on the performance of the MODIS snow-cover mapping algorithm were investigated.

Using both the TM images and the reflectance models, two changes to the current MODIS snow-cover mapping algorithm are proposed that will improve the algorithm's classification accuracy in forested areas. The improvements include using the normalized difference snow index and normalized difference vegetation index in combination to discriminate better between snow-covered and snow-free forests. A minimum albedo threshold of 10% in the visible wavelengths is also proposed. This will prevent dense forests with very low visible albedos from being classified incorrectly as snow. These two changes increase the amount of snow mapped in forests on snow-covered TM scenes, and decrease the area incorrectly identified as snow on non-snow-covered TM scenes. © 1998 John Wiley & Sons, Ltd.

KEY WORDS snow cover; remote sensing; forest canopy

INTRODUCTION

Snow is an important component of the Earth's surface. Compared with other land covers, its areal extent varies dramatically on very short time-scales (hours–months). Its presence affects physical, chemical and biological processes at many spatial scales and has important societal effects. At the global scale, its high albedo strongly influences the Earth's radiation budget (Foster and Chang, 1993).

* Correspondence to: A. G. Klein, Hydrological Sciences Branch, Mail Code 974, Laboratory for Hydrospheric Processes, NASA/Goddard Space Flight Center, Greenbelt, MD 20771, USA. E-mail: Andrew G. Klein (aklein@glacier.gsfc.nasa.gov)

Snowmelt is an important water resource in many areas of the world (Carroll *et al.*, 1989) and heavy, late season snowfalls can cause serious flooding, or less than average yearly snowfalls can lead to water deficits in areas where snowmelt is a significant water resource (Hall, 1988). Because of its importance from both a scientific and resource management standpoint, accurate monitoring of snow cover extent is an important research goal in the science of Earth systems.

Fortunately, snow is amenable to monitoring using satellite remote sensing and there is a long record of Northern Hemisphere snow cover extent from satellite observations. Since 1966, the extent of continental snow cover has been monitored on a weekly basis using NOAA satellites (Matson *et al.*, 1986; Matson, 1991). Global estimates of snow depth and area have been provided by the scanning multichannel microwave radiometer aboard the Nimbus-7 satellite (Foster and Chang, 1993). Currently, snow cover is monitored operationally for the United States on a weekly basis using NOAA AVHRR 1 km data by NOHRSC, the National Operational Hydrologic Remote Sensing Center (Carroll *et al.*, 1989). Snow cover extent for the Northern Hemisphere is produced at much coarser resolution from digitization of the NOAA snow charts using the National Meteorological Center's standard analysis grid in a polar stereographic projection (Robinson *et al.*, 1993).

The moderate resolution imaging spectroradiometer (MODIS), scheduled for launch in 1998 aboard the first NASA earth observing system (EOS) platform, is designed to provide quantitative estimates of numerous geophysical parameters on a global basis (Salomonson *et al.*, 1992). The high spatial resolution and numerous MODIS spectral bands in the 0.4 to 2.5 μm wavelength region will allow more accurate monitoring of snow cover extent on a global basis than is possible with currently operational satellites. A prototype MODIS snow cover mapping algorithm has been developed to map the areal extent of snow on a global basis (Hall *et al.*, 1995).

Development and validation of the MODIS snow-mapping algorithm is difficult since the MODIS sensor is not yet in orbit. In addition, difficulty in obtaining independent measures of snow cover extents for large areas makes validating any satellite-based snow-mapping algorithm problematic. Despite these difficulties, preliminary validation efforts using Landsat Thematic Mapper (TM) and MODIS airborne simulator (MAS) images have been performed. These validation efforts indicate that the classification accuracy of the current MODIS snow-cover mapping algorithm is very high for cover types with low stature or sparse vegetation (e.g. grassland, agricultural lands, tundra).

Good estimates of snow-covered area have been determined for the Sierra Nevada, California, by Rosenthal (1993) and Rosenthal and Dozier (1996) from Landsat TM data. For a Landsat TM scene acquired over the Sierra Nevada on 10 May 1992, Hall *et al.* (1995) demonstrated that the MODIS snow-cover mapping algorithm correctly classified 98% of the pixels identified by Rosenthal (1993) as containing at least 60% snow cover. Figure 1 extends this comparison using the modified algorithm presented by Rosenthal and Dozier (1996) and the 10 May 1992 Landsat TM scene. The current MODIS snow cover algorithm correctly classifies the majority of pixels containing at least 50% snow cover as estimated by the Rosenthal and Dozier (1996) algorithm, and the agreement is better for Landsat TM spatially degraded to the 500 m resolution of MODIS than the full resolution Landsat TM data. Thus the performance of the MODIS snow-mapping algorithm for this test case shows the desired behaviour of a binary classifier in that pixels over 50% are classified as being snow covered while those containing less than 50% snow cover are classified as non-snow covered.

Using MAS images acquired in central Alaska in 1995, Hall *et al.* (in press) estimated forested densities using a method developed by Robinson and Kukla (1985) relating forest density to albedo. In forested areas where the vegetation density was under 50%, the classification accuracy of the current MODIS snow cover mapping algorithm was found to be greater than 96%. However, in areas where the vegetation density exceeded 50%, the classification accuracy of the current snow-mapping algorithm was found to be lower, with 71% of snow-covered forests being mapped as snow.

Accurate mapping of snow in forested areas is a serious problem as forests cover much of the seasonally snow-covered portion of the world. In North America (Figure 2) approximately 40% of the area north of the

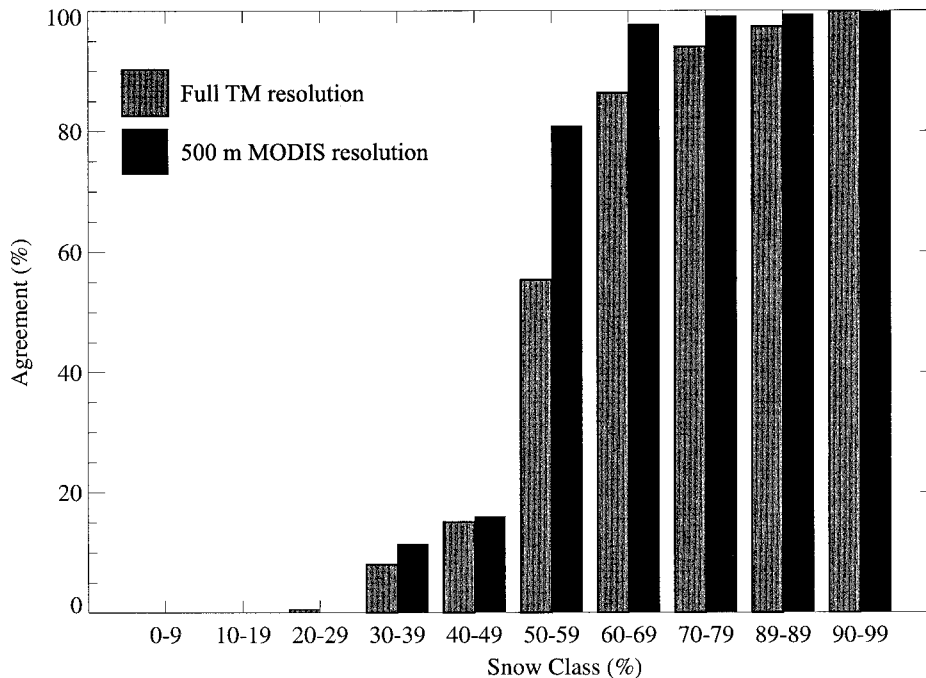


Figure 1. Comparison of the current MODIS snow-mapping algorithm and the snow-covered area algorithm of Rosenthal and Dozier (1996) for a 10 March 1992 Landsat TM scene of the Sierra Nevada, California. The bars indicate the percentage of pixels the MODIS snow-mapping algorithm correctly identified as snow for varying percentages of snow (classes) within the pixel, as identified by the Rosenthal and Dozier (1996) algorithm. Grey bars are the results for a full resolution TM scene and black bars are the results for a TM scene subaveraged to MODIS 500 m resolution

continental snow-line is covered by forests (Table I). Improving classification accuracy in forested areas, and especially in the abundant coniferous forests, represents a key area of improvement in the evolution of the MODIS snow-cover mapping algorithm.

This paper presents an integrated remote sensing and modelling case study that investigates the reflectance changes that forests undergo in the visible to short-wave infrared wavelengths (0.4 to 2.5 μm) owing to the presence of snow on the forest floor. In particular, the effects of snow grain size, solar illumination angle and canopy density on the reflectance of different forest stands are examined and modifications to the prototype MODIS snow-cover mapping algorithm are proposed in order to improve snow mapping accuracy in forests.

Table I. Land cover type percentages for the seasonally snow-covered portion of North America for February snow cover extent

Land cover type	Percentage cover
Agricultural	9.2
Grassland chaparral, shrubland and savanna	10.4
Forests	35.8
Barren or sparsely vegetated	3.8
Tundra	26.0
Perennial snowfields or glaciers	14.8

Land cover percentages were calculated using the Anderson land use and land cover classification modified for the global 1 km land cover characteristics database (Loveland and Belward, 1997) for the area north of the continental snow-line. The continental-scale snow extent is for February.

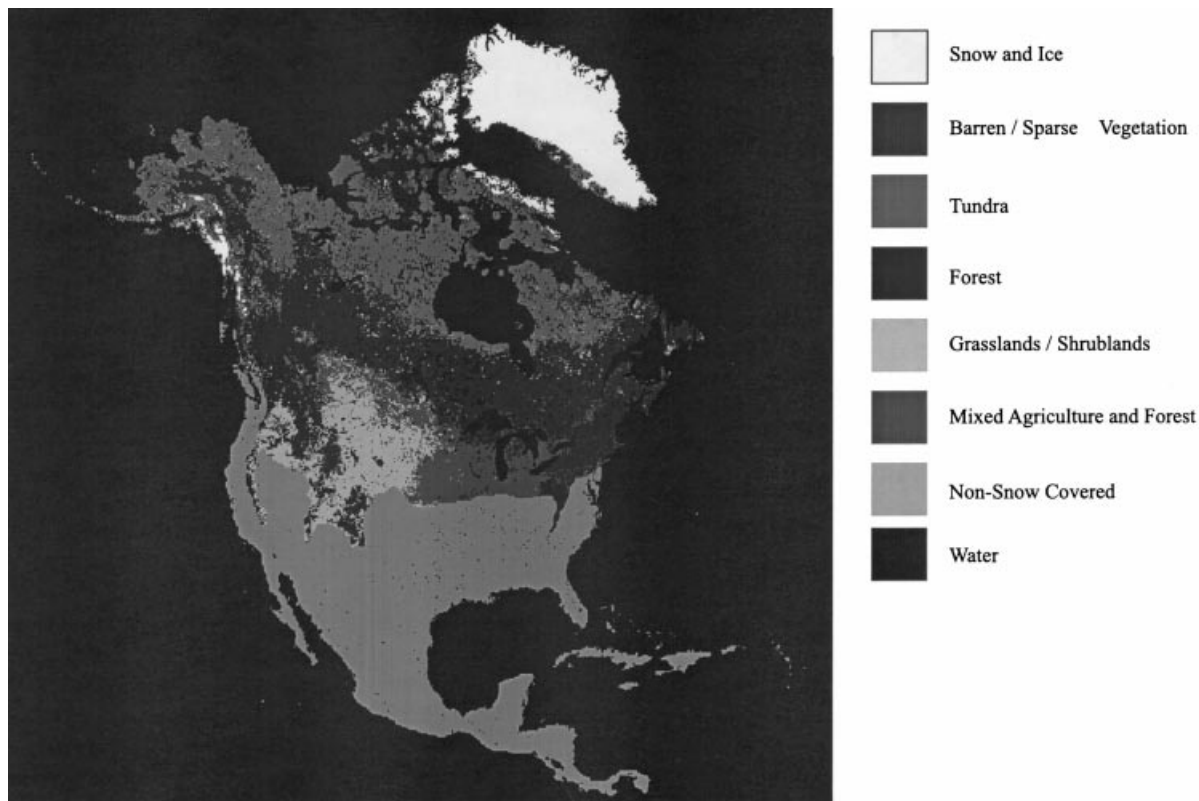


Figure 2. Land cover map for North America. The land cover map is derived from AVHRR imagery and uses the Anderson land use and land cover classification modified for the global 1 km land cover characteristics database (Loveland and Belward, 1997). The continental-scale snow extent for February is shown

STUDY SITE

The southern study area (SSA) of the Boreal Ecosystem–Atmosphere Study (BOREAS) project was selected for this investigation. The excellent characterization of the vegetation from both field and remote sensing studies conducted as part of BOREAS (Sellers *et al.*, 1995) make the area well suited for assessing the effects of vegetation differences on the classification accuracy of the MODIS snow cover mapping algorithm. The SSA (Figure 3) is an approximately 130 km × 90 km area situated north of Prince Albert, Saskatchewan, and is located near the southern limit of the boreal forest (approximately 54°N, 105.25°W). The SSA is characterized by gentle relief and is composed of glacial till plains and rolling or hilly moraines. The SSA contains agricultural lands and boreal forest. Vegetation within Prince Albert National Park, in the western portion of the SSA, is generally characterized by aspen and spruce uplands, black spruce and tamarack bogs, jack pine ridges, sedge meadows and fescue grasslands. In addition, there are uniform stands of aspen and smaller stands of jack pine and black spruce, as well as large tracts of land that have been clear-cut. To the east of the park, the vegetation is mixed boreal forest. On well drained or sandy sites, jack pine dominates, while black spruce dominates poorly drained sites. Mixed stands of aspen and white spruce occur on well-drained glacial deposits. A forest cover map has been developed from the 6 August 1990 Landsat TM scene (shown in Figure 3) by F. G. Hall of NASA/Goddard Space Flight Center. This map serves as the basis for evaluating the performance of the MODIS snow cover mapping algorithm by forest type.

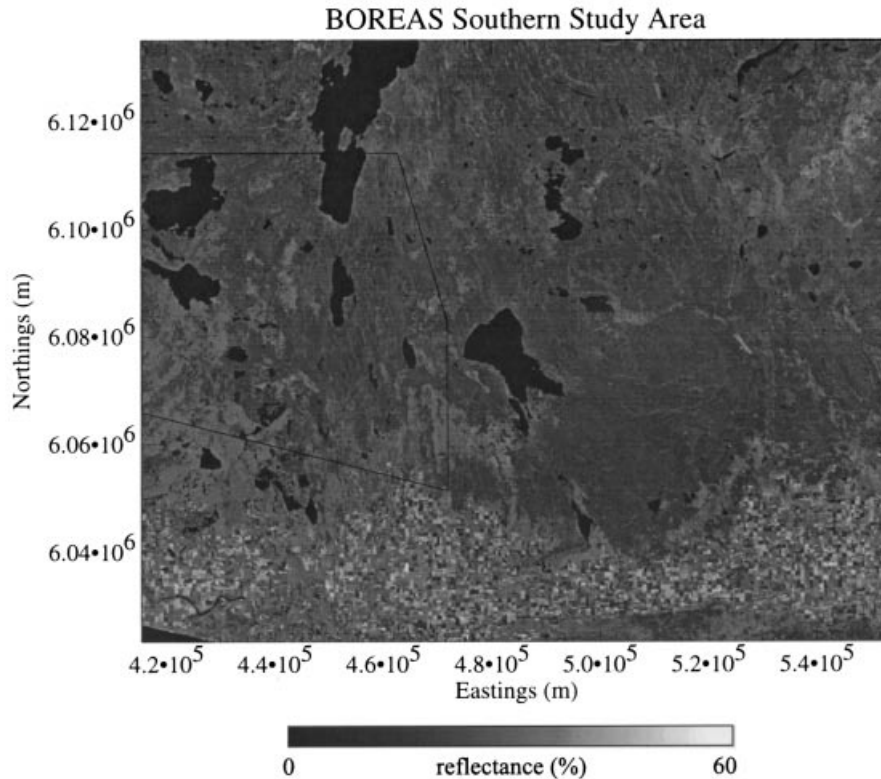


Figure 3. Landsat TM scene (TM band 4) for 6 August 1990 showing the southern study area of the BOREAS project. The outlined area is a cloud-free area from which the snow classification results for all scenes are extracted. The image is in Universal Transverse Mercator (UTM) projection zone (13) and the numbers on the borders are eastings and northings (metres)

MODIS INSTRUMENT CHARACTERISTICS

MODIS is an imaging radiometer with 36 spectral bands in the visible, reflective-infrared and thermal-infrared wavelengths (0.4 to 14.0 μm). MODIS is designed to provide key measurements of the land surface, ocean and atmosphere at regional to global scales on a daily basis. To provide coverage of a large area, MODIS has a large swath width of 2330 km ($\pm 55^\circ$ view angle). However, to minimize distortions in pixel geometry and anisotropic reflectance effects, only data from the portion of MODIS swath covering view angles $\pm 45^\circ$ from nadir will be used in the snow-mapping processes. However, most seasonally snow-covered areas will be imaged daily within the narrower swath (Hall *et al.*, 1995).

Of the 36 MODIS spectral bands, only seven are designed for land surface remote sensing. Some of these bands have the spectral and spatial characteristic suitable for use in the MODIS snow-mapping algorithm (Figure 4). The spatial resolution of MODIS bands 1 and 2 is 250 m, while MODIS bands 3 to 7 have a 500 m resolution.

In order to develop and validate the MODIS snow-cover mapping algorithm prior to launch, Landsat TM has been employed as a MODIS surrogate. With the exception of MODIS band 5 (1.23–1.25 μm), all bands used in the current MODIS snow-cover mapping algorithm have corresponding Landsat TM bands, albeit with wider band passes (Figure 4). The nadir view of Landsat is a limitation, as off-nadir effects are known to affect the accuracy of the MODIS snow cover mapping algorithm, but cannot be simulated using TM data (Hall *et al.*, unpublished data).

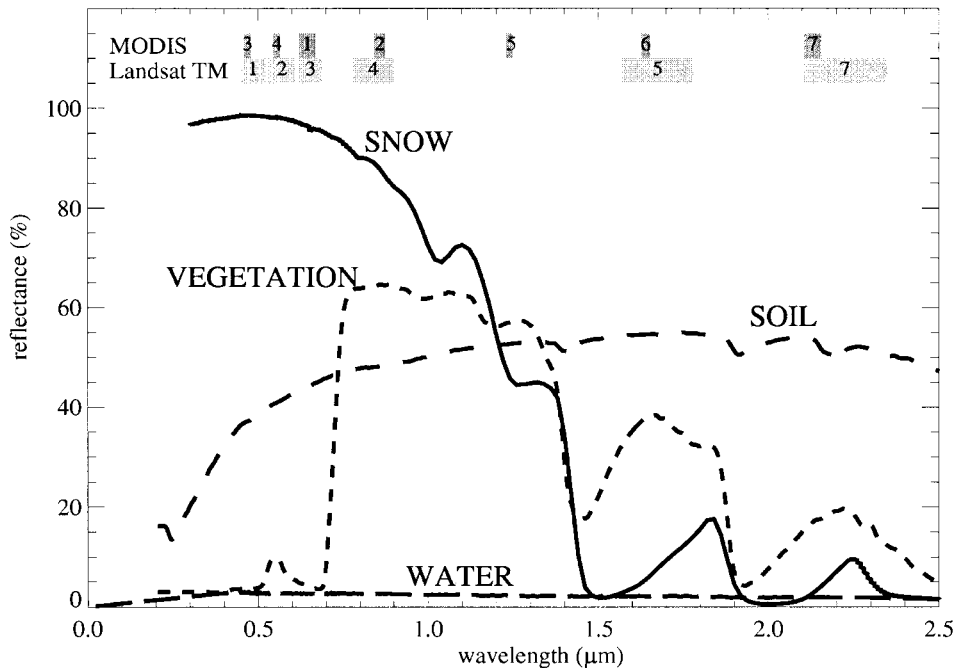


Figure 4. General reflectance curves for snow, soil, vegetation and water. The vegetation and soil curves are derived from the USGS Digital Spectral Library (Clark *et al.*, 1993). The snow and water curves are from the John Hopkins University Spectral Library (Salisbury and D'Aria, 1992, 1994; Salisbury *et al.*, 1994). MODIS land cover band passes and TM band passes are also shown

MODIS SNOW COVER MAPPING ALGORITHM

As currently designed, the MODIS snow-mapping algorithm is a fully automated, computationally frugal algorithm that will be ready to implement by the launch of the EOS AM-1 spacecraft in 1998 (Hall *et al.*, 1995). It builds on nearly two decades of remote sensing research. The algorithm represents a significant improvement over existing operational products because of the ability of MODIS to better discriminate between snow and clouds. Cloud screening will be performed using the MODIS cloud product (Ackerman *et al.*, 1996) prior to snow classification.

The MODIS snow-cover mapping algorithm uses at-satellite reflectances in the 0.4 to 2.5 μm wavelength range to determine if a pixel is snow covered using two classification criteria. The first is a normalized difference snow index (NDSI) value of greater than 0.40. The NDSI value is calculated as

$$NDSI = \frac{MODIS4 - MODIS6}{MODIS4 + MODIS6} \approx \frac{TM2 - TM5}{TM2 + TM5} \quad (1)$$

The high reflectance of snow in the visible compared with the mid-infrared portion of the spectrum (see Figure 4) yields high NDSI values for snow compared with other surface materials. Clouds also tend to have high reflectances in both the visible and mid-infrared wavelengths, so the NDSI also serves as a snow/cloud discriminator. The combination of visible and mid-infrared wavelengths has a long history of use in snow classification (Kyle *et al.*, 1978; Bunting and d'Entremont, 1982; Dozier, 1989). Additionally, only pixels with a reflectance at about 0.9 μm , (MODIS band 2 or TM band 4) of greater than 11% are considered snow. This effectively excludes liquid water that also may have high NDSI values. A complete description of the prototype MODIS snow-cover mapping algorithm is given in Riggs *et al.* (1994) and Hall *et al.* (1995).

METHODOLOGY

In this study, remote sensing observations, a snow reflectance model and a canopy reflectance model are used to examine how the reflectance of snow-covered and snow-free forests differs in the visible to mid-infrared (0.4 to 2.5 μm) wavelengths. In addition, the snow reflectance model and canopy model are used in concert to examine how the reflectance of a snow-covered forest changes as a function of incidence angle, snow grain size, canopy type and percentage canopy cover. The aim of the modelling is to provide a semi-quantitative estimate of how the presence of snow on the forest floor would be expected to alter the reflectance of a forest stand. The modelling is used as an aid in interpretation of Landsat TM images and in developing enhancements to the current MODIS global snow-mapping algorithm. Because of the generalizations required to develop a global algorithm, the goal of the modelling was not to produce exact reproductions of the spectral reflectance measured for a particular stand in the BOREAS study area.

Landsat TM

Prior to analysis, the at-satellite radiances of the five BOREAS Landsat TM scenes (Table II) were converted to at-satellite reflectances following the procedure described in Markham and Barker (1986). No atmospheric correction was performed, since this is not planned for the at-launch MODIS snow-mapping algorithm because an atmospheric correction appropriate for bright targets has not yet been developed. The TM scenes were georegistered into a Universal Transverse Mercator (UTM) projection using ground control points and a second-order polynomial warp, and the area corresponding to the BOREAS southern study area was extracted for analysis.

Table II. Acquisition date, path, row and solar zenith angles of Landsat TM scenes of the BOREAS southern study area used in the study

Acquisition date	Path	Row	Solar zenith angle ($^{\circ}$)
6 August 1990	37	22	42.1
18 January 1993	37	22	77.9
6 February 1994	37	22	73.6
29 March 1995	37	22	55.9
21 September 1995	37	22	57.4

Basic model of the reflectance of a forest stand

If it is assumed that a satellite observation (pixel) of a forest stand is larger than the size of individual trees but smaller than the stand, then the reflectance of the stand can be modelled as a linear combination of four elements and their areal proportions.

$$\rho_{\text{stand}} = C_{\text{sun}}\rho_{C_{\text{sun}}} + B_{\text{sun}}\rho_{B_{\text{sun}}} + C_{\text{shadow}}\rho_{C_{\text{shadow}}} + B_{\text{shadow}}\rho_{B_{\text{shadow}}} \quad (2)$$

where ρ_{stand} is the total stand reflectance; $\rho_{C_{\text{sun}}}$, $\rho_{B_{\text{sun}}}$, $\rho_{C_{\text{shadow}}}$ and $\rho_{B_{\text{shadow}}}$ are the reflectances of sunlit crown, sunlit background, shadowed crown and shadowed background, respectively; and C_{sun} , B_{sun} , C_{shadow} and B_{shadow} are the areal proportions of the four components (Li and Strahler, 1986; Woodcock *et al.*, 1997; Huemmrich, 1995).

In this framework, the contribution of a snow cover lying on the forest floor to the stand reflectance is represented by the sum of the two background terms in Equation (2). The contribution of snow to the stand reflectance depends on the reflectance of the snow itself, the fraction of canopy cover and the solar illumination angle, which determines the proportion of sunlit to shadowed snow within the stand.

GeoSAIL, a relatively simple reflectance model for discontinuous canopies, was used to determine the crown reflectances, the fraction of each of the four components within the stand and the transmittance

through the canopy. Reflectances for the sunlit snow are calculated using the Wiscombe and Warren (1980) model, while reflectances for other backgrounds are taken from direct measurements.

In many areas, a Landsat TM pixel, or in the future the much larger MODIS pixel, will not contain only a pure forest stand. To investigate how well the MODIS snow-mapping algorithm performs on these mixed pixels, simple linear mixing of individual components was used to synthesize the spectra of these mixed pixels.

SNOW REFLECTANCE MODELS

The reflectance of snow in the visible to mid-infrared wavelengths depends on the bulk optical properties and geometry of the ice crystals comprising the snowpack and the optical properties of any impurities or liquid water found within the snowpack (Dozier, 1989). Using radiative transfer theory, the reflectance of a snowpack has been successfully modelled (e.g. Bohren and Barkstrom, 1974; Warren, 1982). Snowpacks comprised of both pure snow (Wiscombe and Warren, 1980) and snow with impurities (Warren and Wiscombe, 1980) have been successfully modelled.

In this study, a deep snowpack composed of pure snow is assumed. Snow reflectances for wavelengths ranging from 0.25 to 2.5 μm are calculated for a variety of grain sizes (modelled as the grain radius for the optically equivalent sphere) and illumination angles using the Wiscombe and Warren (1980) model and the Meador and Weaver (1980) hybrid approximation to the two-stream radiative transfer equations. These models calculate a directional hemispherical reflectance (spectral albedo) that differs from the Landsat TM bidirectional reflectance measurements. Despite the failure of these models to account for the anisotropic effects known to affect snow reflectance (Dozier *et al.*, 1988), they do generally match measured spectra (e.g. O'Brien and Munis, 1975). Because the current MODIS snow mapping algorithm does not correct the measured at-satellite radiances for atmospheric or topographic effects, the use of a more complex discrete-ordinate radiative transfer model to calculate snow bidirectional reflectances (e.g. Fily *et al.*, 1997) was considered unnecessary. The two-stream models accurately produce the major features of snow reflectance (high visible and low mid-infrared reflectances) most likely to enable snow-covered and snow-free forests to be distinguished on a global basis.

In addition to pure snow, backgrounds composed of pure snow and leaf litter were considered. A snow-litter background was created by linearly mixing pure snow spectra with leaf litter spectra (Hall *et al.*, 1992).

THE GeoSAIL MODEL

The GeoSAIL model was used to model the three major species found in the BOREAS SSA: black spruce (*Picea glauca*), jack pine (*Pinus banksiana*) and aspen (*Populus tremuloides*). The parameterizations used for each species are shown in Table III and were determined from field measurements conducted in the Superior National Forest (Hall *et al.*, 1992) which is similar in species composition to the SSA. The reflectances of the leaf litter background were also measured (Hall *et al.*, 1992). Snow reflectances that served as the sunlit background were calculated for snow grains with radii ranging from 50 to 2500 μm as described above.

The GeoSAIL model was designed to be an easily parameterized and computationally simple canopy model. It has been successfully used to simulate the spectral reflectance and absorption of photosynthetically active radiation in discontinuous canopies (Huemmerich, 1995). GeoSAIL utilizes the scattering from arbitrarily inclined leaves (SAIL) model (Alexander, 1983; Verhoef, 1984) to calculate the radiative transfer within a tree canopy and the Jasinski geometric model (Jasinski and Eagleson, 1989, 1990) to combine the SAIL calculations into a stand reflectance.

The Jasinski model calculates the areal proportions in Equation (2) for the limiting case where the shadows cast by vegetation are small relative to the size of the area observed. In the model, a forest stand is composed of geometric solids (trees) scattered over a plane with a Poisson distribution. These solids all have the same size and shape and are small compared with the size of the pixel. They cast shadows on the

Table III. GeoSAIL model parameterization

	Height to width ratio	Leaf area index for 100% canopy cover	Canopy components ^{a,b}	Background ^a
Aspen	89.0	1.0	Twigs (A25HB1RF) — 100 or 85% Leaves (A25H29RF, A25H29TF) — 0 or 15%	Leaf litter (BL00201R)
Black spruce	7.0	4.0	Needles (SY2R, SY2T) — 85% Twigs (PM0B201R) — 10%	Leaf litter (BL00201R)
Jack pine	5.5	4.0	Needles (PBLR, PBLT) — 90% Twigs (PB0B201R) — 10%	Leaf litter (BL00201R)

^aNumbers in parentheses indicate the sample identification number in Hall *et al.* (1992) from which the reflectance and transmittance values were obtained. There is no transmittance through twigs or the background.

^bSpherical and planophile leaf angle distributions were used for needles or leaves and twigs, respectively.

background but not on each other. With these constraints, and for a nadir view, the fraction of the pixel that is shadowed background is calculated as

$$B_{\text{shadow}} = 1 - C_{\text{total}} - (1 - C_{\text{total}})^{(\eta+1)} \quad (3)$$

where B_{shadow} is the fraction of shadowed background and C_{total} is the fraction covered by the solid, or the total canopy cover ($C_{\text{sun}} + C_{\text{shade}}$). η is the ratio of canopy cover to shadow area for a single geometric solid and can be calculated for a number of different shapes. It is dependent both on the geometric form and the solar illumination angle. In this study, cones were used to represent black spruce, cylinders were used to represent leafless deciduous trees and both cylinders and cones models were run for jack pine.

For cylinders, η is determined by the height/width ratio of the cylinder (R) and the solar zenith angle (θ)

$$\eta = R \tan(\theta) \quad (4)$$

and for cones

$$\eta = \frac{[\tan(\beta) - \beta]}{\pi} \quad (5)$$

where β is a function of the cone's aspect ratio (ψ) and the solar zenith angle (θ)

$$\beta = \arccos\left[\frac{\tan(\psi)}{\tan(\theta)}\right] \quad (6)$$

For cylinders, the fraction of shadowed canopy (C_{shadow}) is 0 while for cones, whose aspect ratio is less than the solar zenith angle, C_{shadow} is

$$C_{\text{shadow}} = \frac{\beta}{\pi} \quad (7)$$

Illuminated background (B_{sun}) can then be calculated based on the fractions of total canopy (C_{total}) and shadowed background (B_{shadow}) as

$$B_{\text{sun}} = 1 - (C_{\text{total}} + B_{\text{shadow}}) \quad (8)$$

The reflectances of each of the components in Equation (2) are calculated as follows. Sunlit canopy ($\rho_{C_{\text{sun}}}$) is the SAIL model reflectance for a single tree at the specified leaf area index (LAI). Illuminated background

($\rho_{B_{\text{sun}}}$) is the background used in the SAIL model and for snow it is calculated by the snow reflectance model. The two background reflectances ($\rho_{C_{\text{shadow}}}$ and $\rho_{B_{\text{shadow}}}$) are simply the two illuminated reflectances multiplied by the canopy transmittance calculated by the SAIL model. For leafless deciduous trees, the SAIL model cannot calculate a transmittance directly so the shadowed reflectance was arbitrarily calculated as one-third of the illuminated reflectance. While this simplification neglects spectral variations, it nevertheless is a reasonable value (Rosenberg *et al.*, 1983).

LINEAR MIXING MODEL FOR MIXED PIXELS

To investigate the effects of several surface types occurring within a single pixel, a simple linear mixture model was used to create the spectra of a 'mixed' pixel for varying percentages of water, snow and canopy. In this mixing model, the reflectance of the pixel in each band is simply a linear summation of the reflectance of each component multiplied by its areal fraction. This mixing is meant to represent pixels composed of forest stands, open fields covered with snow and small lakes, ponds or wetlands containing open water. The validity of linear mixing in snow-covered areas is discussed by Rosenthal and Dozier (1996). GeoSAIL canopy reflectances for stands with a leaf area index of 4, for spruce and jack pine canopies, and 1, for a leafless aspen canopy, were used for the canopy contribution. Snow reflectances from the Wiscombe and Warren (1980) model were used to represent the snow contribution, and the reflectance of tap water (Salisbury and D'Aria, 1992, 1994) was used to represent the water component. It is recognized that the reflectance of water will vary considerably depending on sediment and chemical composition; however, the characteristic low reflectance of water throughout the wavelengths of interest is captured in this water spectrum. Two separate cases were examined: (1) the background under the canopy and in open areas was pure snow; and (2) the background under the canopy and in open areas was composed of 60% pure snow and 40% leaf litter.

RESULTS AND DISCUSSION

Both the satellite observations and modelling results show that a forest stand will undergo changes in reflectance as snow covers other surface materials on the forest floor such as moss or leaf litter. Changes in the reflectance of a forest stand observed in Landsat TM images can be successfully modelled using the relatively simple scheme described above. The modelling provides a theoretical basis for understanding these reflectance changes and also serves as a basis for suggesting changes to the current implementation of the MODIS snow-cover mapping algorithm.

Observed reflectance changes

Several changes occur in the spectra of a deciduous or coniferous forest stand as it becomes snow covered that can be explored in the MODIS snow-mapping algorithm (Figure 5). The primary change in reflectance occurs in the visible wavelengths, as snow has a much higher visible reflectance than soil, leaves or bark. Depending on the vegetation type, snow may also cause a decrease in the mid-infrared reflectance of the stand. The increase in visible reflectance and decrease in mid-infrared reflectance has been used as a discriminator both between snow and other surface covers and between snow and clouds by numerous authors (Kyle *et al.*, 1978; Bunting and d'Entremont, 1982; Dozier, 1989). This behaviour is captured in the normalized difference snow index.

As can be seen in Figure 5, the reflectances of snow-covered forests in the visible wavelengths (TM bands 2 and 3) are *c.* 16% for coniferous canopy and *c.* 23% for deciduous canopy. The low visible reflectances for TM bands are in agreement with broadband albedo measurements of jack pine stands in winter, where the mean daily albedo was found to fluctuate between 12 and 17% (Harding and Pomeroy, 1996; Pomeroy and Dion, 1996). The higher reflectances observed in TM band 1 are probably caused by the lack of an atmospheric correction. Because band 1 suffers most from atmospheric effects, it is not used in the MODIS snow-cover mapping algorithm. Winter at-satellite reflectances from Landsat TM, and in the future from

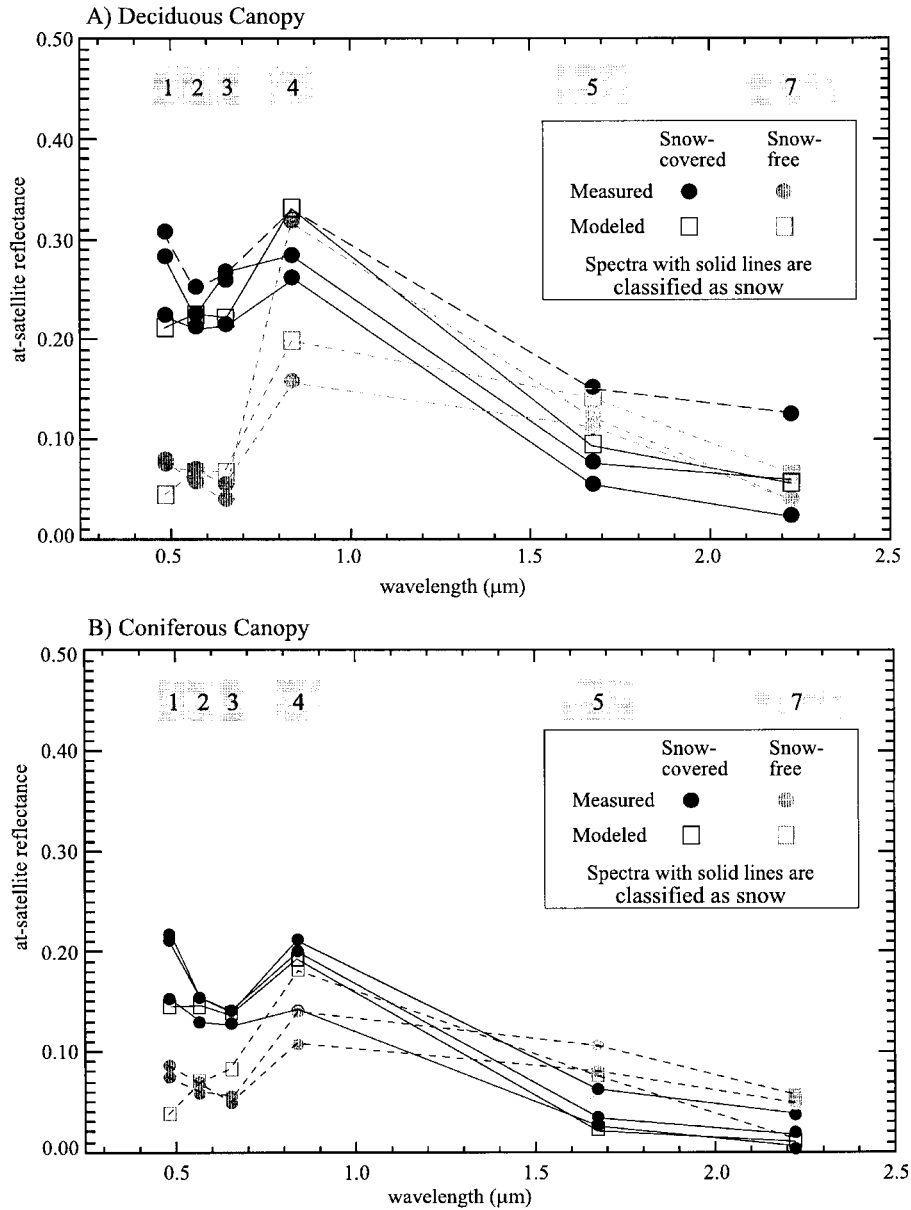


Figure 5. (A) Observed and modelled spectra for deciduous sites in the BOREAS study area. Circles represent the average spectra from a 5×5 pixel area from each of the five TM scenes in Table II. The black circles and lines are spectra from the three winter scenes and grey circles and lines are spectra from the two summer scenes. Solid black lines indicate that the spectra meets the classification criteria for snow in the original MODIS snow cover mapping algorithm. Boxes indicated the modelled reflectance for a leafless aspen stand for summer (grey) and winter (black) conditions. (B) As (A) except for a jack pine coniferous forest

MODIS, will also be higher than those measured at low levels over the canopy because part of the signal received at the satellite is derived from snow cover that is visible in gaps between forest stands.

The other fundamental change that snow causes in the spectral response of a forest, which can be exploited in a global algorithm, is that the reflectance in the visible will often increase with respect to the near-infrared reflectance. This behaviour is captured in the normalized difference vegetation index (NDVI), as snow will

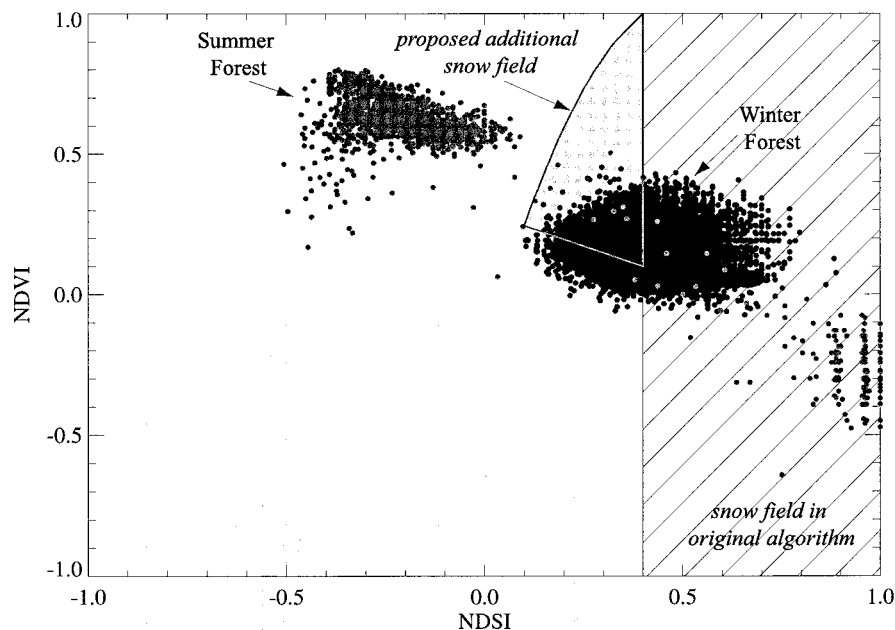


Figure 6. NDSI versus NDVI plot for coniferous and deciduous forest stands within the BOREAS study area. Grey values are from the 6 August 1990 TM scene and black values are from the 6 February 1994 scene. The hatched area shows the present NDSI values considered to be snow in the current algorithm, while the grey shaded region represents the proposed field for capturing snow-covered forests in the MODIS snow-cover mapping algorithm

tend to lower the NDVI. This behaviour has been previously noted in AVHRR imagery (K. F. Huemmerich, personal communication).

Taken together, the NDVI and NDSI provide a strong signal that can be exploited to classify snow-covered forests. Shown in Figure 6 is a plot of NDSI versus NDVI values derived from the Landsat images for coniferous and deciduous sites in winter and summer. A clear difference exists between the summer and winter values. However, the current NDSI threshold of 0.4 used to map snow (hatched area in Figure 6) fails to capture this difference. An additional field (light grey in Figure 6) can be used as an additional criteria test in the MODIS snow cover mapping algorithm.

The position of these classes in the NDSI–NDVI space can be explained by examination of the generic spectra shown in Figure 4. As snow has a high reflectance ($\geq 95\%$) in the visible (TM band 2) and low reflectance ($\geq 10\%$) in the mid-infrared (TM band 5), a pixel containing only snow would be expected to have a NDSI value of 0.80 or greater. As the reflectance of snow in the near-infrared (TM band 4) is similar to or slightly less than its reflectance in the red (TM band 3), snow would be expected to have a NDVI value slightly less than 0.0.

The mid-infrared reflectance of soil is generally higher than its visible reflectance and thus would be expected to have a NDSI of less than 0.0. The near-infrared reflectance of soil is only slightly greater than that in the visible so soil should have a NDVI equal to or slightly greater than 0.0. As the fraction of snow in an otherwise soil-covered pixel increases, a large increase in NDSI, but relatively little change in the NDVI, would be expected.

For the case of mixed snow/forest pixels, however, much smaller changes occur in the NDSI. This is due to the similar reflectance of snow and vegetation in the mid-infrared wavelengths, making changes in the NDSI primarily a result of reflectance changes in the visible wavelengths. However, there is a large change in the NDVI as well, as the presence of snow will decrease the NDVI values from 0.4–0.8 to near 0.0. Together, changes in NDVI and NDSI can be used to separate snow-covered from snow-free forests.

GeoSAIL modelling

While it is evident from analysis of Landsat TM of the BOREAS site that snow-covered and snow-free forests can be distinguished on the basis of their NDSI and NDVI values, the range of values expected under the entire range of canopy, snow and illumination conditions encountered in a global mapping programme cannot be determined from a handful of Landsat TM scenes. To address this shortcoming, the GeoSAIL model was used to model vegetation reflectances under a suite of environmental conditions. These calculations are used to understand the processes operating in a snow-covered forest and to help determine the classification criteria needed to distinguish successfully between snow-covered and snow-free forests.

Spectra generated for both deciduous and coniferous species from the GeoSAIL model compare well with the observed spectra extracted from the Landsat TM scenes based on the vegetation map (Figure 5). However, the GeoSAIL spectra for the coniferous species that are most similar to the observed spectra are those for canopy cover percentages lower than is typical of the BOREAS sites.

The magnitude of the reflectances calculated for coniferous species also appears to be too low in all wavelengths for large solar zenith angles (generally $\geq 60^\circ$). In fact, the modelled reflectances for spruce with canopy cover greater than 50% and solar zenith angles greater than 60° are seldom higher than 10% in any band. Thus, while the shape of the spectral curve matches the observed shape, the overall magnitudes are too low. Very low reflectances at high solar zenith angles are consistent with observations made at a jack pine site in the SSA by Pomeroy and Dion (1996). The higher measured reflectance values suggest that a portion of the signal received at the sensor may be derived from snow visible between forest stands.

For high illumination angles, the canopy intercepts nearly all radiation reaching the forest floor and the resulting reflectances are very low. Additionally, the spectral character of the radiation is strongly influenced by the needle transmittance. Because needle transmittance is much higher in the near-infrared (35–40%) and the mid-infrared (*c.* 15%) compared with the visible ($< 8\%$), NDVI values tend to be higher and NDSI lower than would be expected. Despite these problems, the GeoSAIL model spectra capture the major reflectance changes in a forest stand between snow-free and snow-covered conditions.

The NDSI–NDVI plots generated by the GeoSAIL model (Figure 7) are consistent with the observations. As the canopy cover increases, the snow-free and snow-covered NDSI–NDVI values converge because the current model neglects seasonal changes in canopy phenology. Despite the limitations in the model, it is clear that the reflectance of snow-free and snow-covered forests would be expected to differ, and these modelled differences are consistent with those observed in the TM scenes from the SSA.

The GeoSAIL model was also used to predict the changes in the reflectance of a snow-covered forest resulting from changes in grain size and illumination angle. Changes in the reflectance of the snow-pack and solar illumination angle affect coniferous and deciduous forests quite differently. This is not surprising as it is well known that forest type is important in the remote sensing of forests (e.g. Woodcock *et al.*, 1997).

Varying grain size causes the greatest changes in NDSI and NDVI values at the lowest canopy cover percentage. As canopy cover increases, the effects of grain size differences disappear. Decreasing grain size will cause substantial lowering in the NDSI, but only small changes in the NDVI. Thus, in an NDSI–NDVI plot, grain size changes may be identified by migration along the NDSI axis, as can be seen for the pure snow points in Figure 7.

Illumination angle effects are more complicated and vary considerably between deciduous and coniferous species. At low canopy cover percentages, increasing the illumination angle decreases the NDSI in much the same way, as does decreasing grain size. However, this range is much less than for changes in snow grain size. For aspen, the effect of illumination angle decreases quickly as the canopy cover increases. In the two coniferous species and for high illumination angles, the NDSI and NDVI values are similar to those for a complete canopy closure, even for relatively low percentages of canopy cover. This is due, in part, to the problems with transmittance through the canopy, as discussed above.

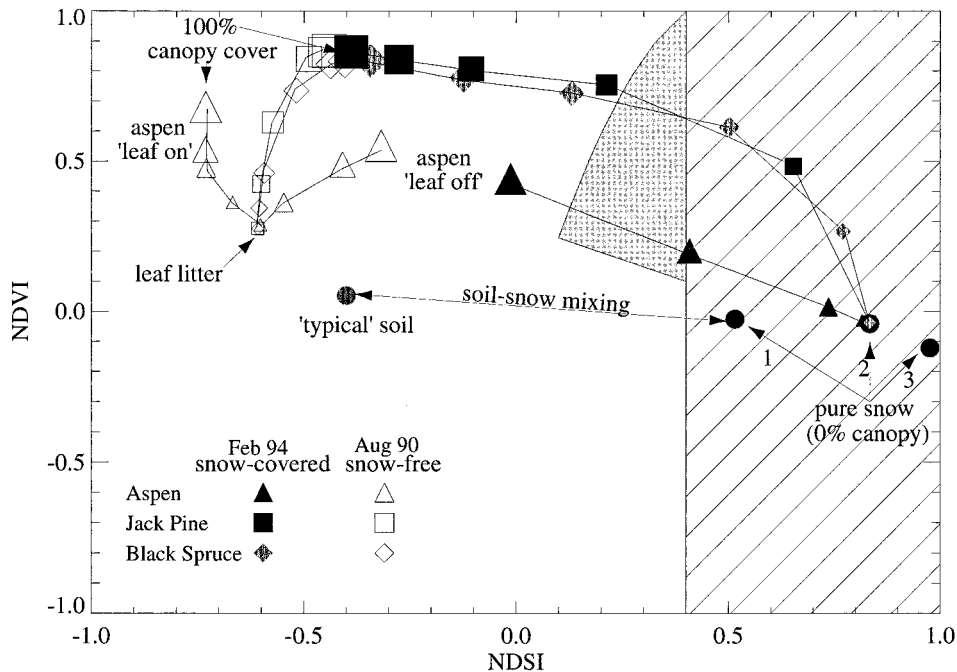


Figure 7. NDSI versus NDVI plot for modelled aspen (triangle), jack pine (square) and spruce (diamond) stands. The filled symbols represent snow-covered conditions and open symbols represent snow-free conditions. Increasing symbol size represents increasing leaf area index (% canopy cover) of the modelled stand. Thus small symbols indicate NDSI–NDVI values near those of pure snow or pure leaf litter, while the largest symbols are values corresponding to those for a more complete canopy. The hatched area shows the present NDSI values considered to be snow in the current algorithm, while the grey shaded region represents the proposed field for capturing snow-covered forests in the MODIS snow cover mapping algorithm. The dark circles represent the NDSI–NDVI values for pure snow of three grain sizes (1) 50 μm , (2) 250 μm and (3) 2500 μm . The illumination angles corresponding to the 6 February and 6 August TM scenes were used

Illumination angle changes affect coniferous and deciduous species stands differently both because of reflectance and transmittance differences and because of the differing geometry of the species. For sparse aspen stands, the fraction of shadowed background increases linearly with illumination. For dense canopies, except for the lowest illumination angles, most of the background is shadowed (Figure 8). The shading effects of coniferous species are quite different. For sparse canopies, the background is mostly sunlit, but as the percentage of canopy cover increases in a stand, the behaviour becomes more like that of deciduous trees (Figure 8).

The GeoSAIL model was also used to help determine the causes of classification errors in the MODIS snow-cover mapping algorithm. For instance, Hall (unpublished data) previously noticed that less snow was mapped in deciduous stands in the 6 February 1994 TM scene compared with the 18 January 1993 TM scene, however, he was unable to explain the differences adequately although he did propose that the small change in solar zenith angle (*c.* 4°) may account for the difference. Examination of a scatter plot of NDSI–NDVI for both dates shows that NDSI values for the 6 February scene are shifted to lower values compared with 18 January. The GeoSAIL results imply that such a shift is consistent with either a change in solar zenith angle or in grain size. However, analysis of the GeoSAIL results shows that the change in NDSI values for this solar zenith angle difference is probably too small to account for the observed shift. This suggests that snow grain sizes on the two dates may differ. Significant changes in the mid-infrared reflectance observed on snow-covered lakes in the area also occur between the two dates. This also discounts differential shadowing between the two dates as a possible cause of the observed differences.

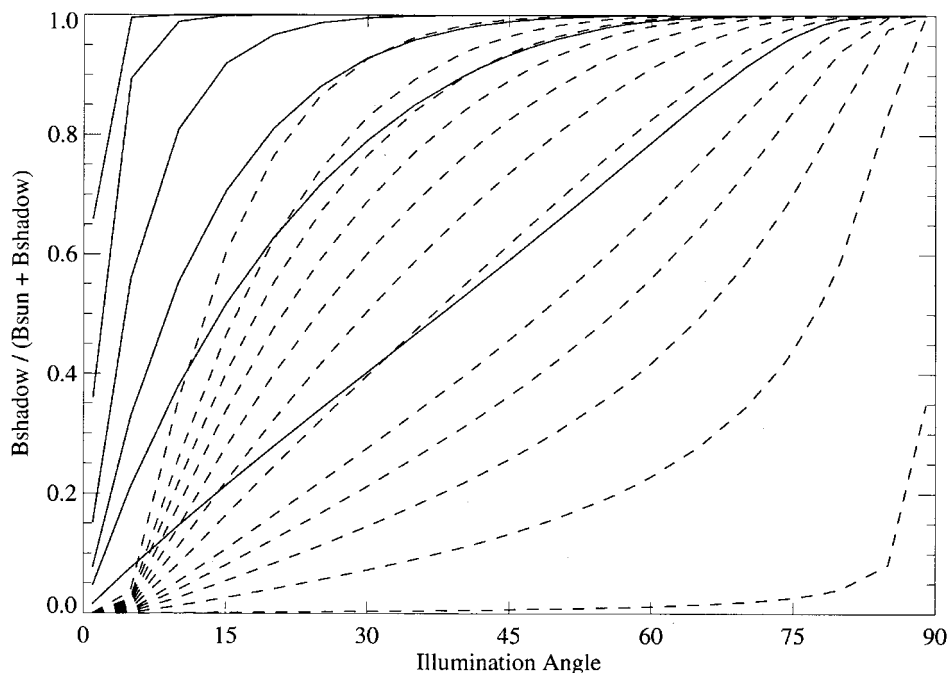


Figure 8. Shaded background fraction as a function of solar zenith angle for aspen (solid) and black spruce (dashed) stands

PROPOSED CHANGES TO THE CURRENT SNOW MAPPING ALGORITHM

Addition of the NDSI–NDVI threshold field

The remote sensing observations and modelling results indicate that NDSI and NDVI values effectively delineate snow-free and snow-covered forests. This is incorporated into the current MODIS snow-cover mapping algorithm in the following manner. An additional criteria test incorporating NDSI and NDVI values is used to classify snow-covered forest pixels. The field boundary is based on TM observations and the GeoSAIL model. Pixels falling in the resulting field (shown in grey in Figures 6 and 7) are considered to be snow.

This new field is designed to capture as much of the variation in NDSI–NDVI values observed in the snow-covered forests as possible, while minimizing inclusion of non-forested pixels. It was designed to include forest-covered pixels that have NDSI values lower than the current threshold, yet have NDVI values lower than would be expected for snow-free conditions. The decision boundary at the low NDVI values was designed to exclude, to as large an extent as possible, pixels containing a mix of snow and soil (e.g. cropland, prairie) which tend to mix along a line below this threshold.

Addition of band 2 threshold

One additional problem occurs in the detection of snow under certain forest types. Many forest types, most notably black spruce, have very low reflectances in the 1.6 μm wavelength (TM band 5). These low reflectances cause the denominator in the NDSI to be quite small and only small increases in the visible wavelengths (TM band 2) are required to make the NDSI value high enough to make a pixel be classified as snow. For instance, if the mid-infrared reflectance is 5%, which is not uncommon for large solar zenith angles and coniferous canopies, then it may only take a visible reflectance of 12% to make the NDSI exceed the 0.40 threshold. The problem is exacerbated when the new NDSI–NDVI threshold is employed, since lower NDSI values will be classified as snow.

To limit errors of commission in the revised MODIS snow cover mapping algorithm, a visible threshold will be employed to prevent pixels with very low visible reflectances from being classified as snow as has previously been suggested by Dozier (1989). Here, a threshold of 10% in TM band 2 was used. Landsat TM band 2 was selected over band 1 because of the greater effects of Rayleigh scattering at shorter wavelengths. The addition of a visible threshold significantly reduced the number of pixels in the summer scenes classified as snow (Table IV) and provided more consistent classification of snow in forests in the winter scenes.

Comparisons of the MODIS snow cover mapping algorithm

The modified snow-mapping algorithm incorporating the two modifications described above and the current algorithm were run concurrently on the spectra generated from the GeoSAIL and linear mixing models, as well as the five BOREAS scenes. These comparisons were done to determine if the proposed changes provided any improvements over the original algorithm.

Model comparison

The snow-mapping algorithms were run on spectra generated from both the GeoSAIL model and the linear mixing model to see if the changes allow for better mapping of snow both for pixels composed of pure forest stands and mixed pixels. Figure 9 presents results for the pure stand case for a solar zenith angle of 60° and varying mixtures of snow and leaf litter. While neither algorithm maps a pixel as containing snow where it comprises less than 50% of the background or is at high canopy cover percentages, the revised algorithm does offer some small improvements over the current algorithm, particularly in the case of aspen. It is interesting to note that in the case of the modelled spruce stand, the current snow-mapping algorithm will classify spruce stands as containing snow for higher canopy percentages than does the revised algorithm (filled diamonds). This is a direct effect of the addition of the 10% threshold in the green (MODIS band 4 and TM band 2) which will prevent these stands with very low visible albedos from being mapped as snow.

While the algorithm revisions would appear to offer little in the way of improving the performance for pixels composed of pure forest stands, few 500 m MODIS pixels will be composed solely of pure forest stands. As can be seen in the ternary diagrams shown in Figure 10, the algorithm revisions allow for much improved mapping of snow in mixed pixels. For the case where the background is comprised of pure snow, both in open fields and under the forest canopy, both algorithms are able to map a pixel as containing snow even if snow comprises only a small fraction of the pixel. However, the revised algorithm will, in the case of aspen and jack pine, map a pixel as snow under more combinations of vegetations/open/water than does the current algorithm. The improvement of the revised algorithm over the current algorithm is even greater for the case where the background is composed of 60% snow and 40% leaf litter.

The results of running the MODIS snow-mapping algorithms on model-generated spectra suggest that the revised algorithm may provide slightly improved mapping of pixels composed of pure forest stands and greatly improved mapping of pixels containing a mix of cover types.

Landsat Thematic Mapper comparison

While model-generated spectra can give some idea of the relative performance of the two algorithms under varying conditions, the true test is with actual image data. The revised snow mapping algorithm and the current algorithm were also run on the five Landsat TM scenes of the BOREAS SSA listed in Table II. Because variable cloud cover occurs in several of the scenes, only a portion of the BOREAS southern study area was used for comparison and is outlined in Figure 3. The vegetation map was used to subdivide the region by cover type so that a comparison of the current and revised snow-mapping algorithms by vegetation type could be made using the Landsat data.

Because validation of actual snow cover extent for the entire area was not possible, either through field observations or aerial photography, two simplifying assumptions are required. The first is that snow cover is assumed to be 100% in the winter and spring scenes (18 January 1993, 6 February 1994 and 29 March 1995) and snow cover is assumed to be 0% for the summer and autumn scenes (06 August 1990 and 21 September

Table IV. Mapping accuracy of the revised MODIS snow-mapping algorithm. The first column for each date indicates the percentage of each cover type mapped as snow while values in parentheses indicate the percentage change in area mapped from the original algorithm. Positive values indicate more area mapped as snow, negative values less area mapped as snow. Also shown is the total area for each cover type

	18 January 1993	6 February 1994	29 March 1995	6 August 1990	21 September 1995	Area (km ²)
Wet conifer	99.91 (0.27)	91.60 (15.84)	89.26 (-1.29)	0.00 (0.00)	0.10 (0.00)	1323.3
Dry conifer	99.98 (0.12)	93.25 (10.44)	96.35 (0.76)	0.15 (-0.07)	0.15 (0.02)	10.1
Mixed	99.73 (1.41)	86.11 (37.36)	87.33 (14.75)	0.00 (0.00)	0.00 (-0.04)	536.9
Deciduous	99.61 (1.64)	56.59 (33.86)	89.36 (6.29)	0.00 (0.00)	0.00 (0.00)	373.2
Fen	99.85 (0.28)	82.86 (20.01)	91.97 (5.01)	0.00 (0.00)	0.00 (-0.02)	46.5
Water/lake ice	100.00 (0.01)	99.80 (0.46)	99.91 (0.02)	0.00 (-0.01)	0.00 (0.00)	367.2
Disturbed	99.97 (0.11)	96.87 (10.04)	99.06 (0.81)	0.00 (0.00)	0.01 (0.00)	46.0
Young regrowth	99.99 (0.00)	98.54 (2.99)	99.48 (0.13)	0.00 (0.00)	0.00 (0.00)	41.8
Medium regrowth	99.95 (0.14)	79.47 (10.36)	98.56 (0.78)	0.00 (0.00)	0.01 (0.00)	98.9
Older regrowth	99.94 (0.13)	87.92 (11.51)	97.92 (1.30)	0.00 (0.00)	0.01 (-0.01)	108.6
Visible burn	99.99 (0.01)	70.16 (2.44)	98.84 (0.24)	0.00 (0.00)	0.00 (-0.01)	13.1
Average	99.90 (0.41)	85.74 (14.11)	94.92 (2.61)	0.014 (-0.01)	0.03 (-0.01)	Total: 2965.6

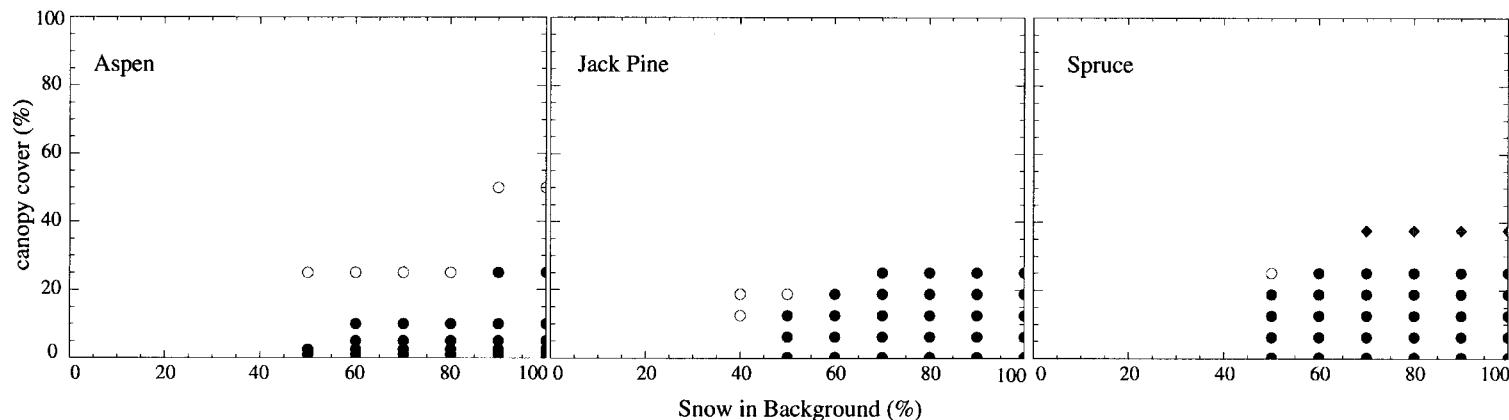


Figure 9. Comparison of the current and proposed MODIS snow mapping algorithms for aspen, jack pine and spruce canopies. For each canopy type, the results of the snow cover classifications are shown for differing fractions of snow versus leaf litter and for varying amounts of canopy cover. Filled circles indicate conditions where both algorithms classify the modelled stand as snow, open circles only the revised algorithm and filled diamonds only the original algorithm. The results are for a solar zenith angle of 60° and the grain size (radius of optically equivalent sphere) of 250 μm

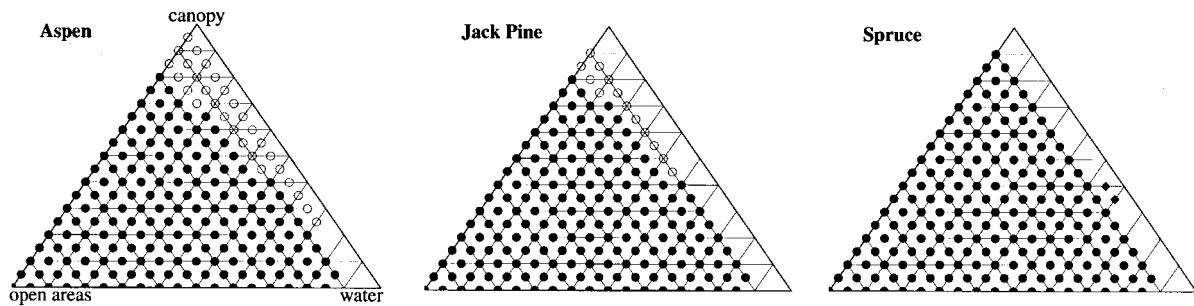
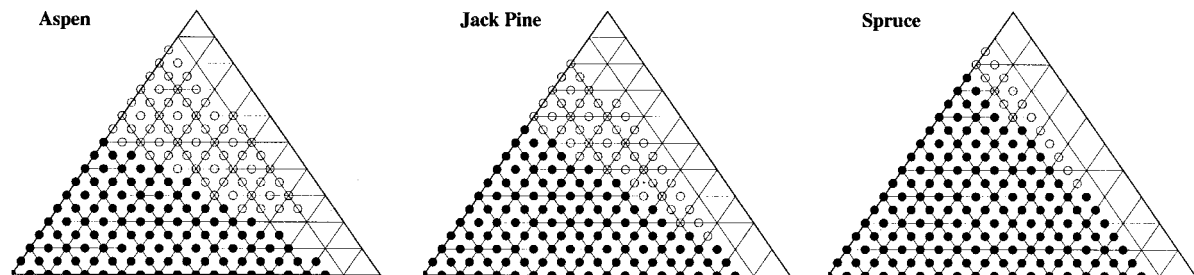
A) background: Pure Snow**B) background: 60% Snow & 40% Leaf Litter**

Figure 10. Ternary plots showing the classification from mixed pixels for (A) a background of pure snow and (B) a background of 60% pure snow and 40% leaf litter for three canopy types. Each location in the ternary diagram represents a different percentage mix of canopy, open areas and water. Filled circles indicate conditions where both algorithms classify the modelled pixel as snow, open circles only the revised algorithm and filled diamonds only the original algorithm. The results are for a solar zenith angle of 60° and the grain size (radius of optically equivalent sphere) of $250 \mu\text{m}$

1995). Analysis of the Northern Hemisphere weekly snow cover and sea ice dataset obtained from the EOSDIS NSIDC Distributed Active Archive Center (NSIDC DAAC), University of Colorado, Boulder, shows that snow-covered conditions persisted in the area for at least three weeks after the acquisition of each winter TM scene. This lends support to the assumption that 100% snow cover existed at the time the three winter scenes were acquired. With these two assumptions a quantitative comparison of the accuracy of the modified and current MODIS snow-cover mapping algorithms is possible.

The proposed modifications increase the percentage of snow mapped in the winter scenes and decrease the percentage incorrectly mapped as snow in the summer and autumn scenes (Table IV). In the winter scenes, the greatest increases in the percentage of pixels mapped as snow occur in the forests (wet conifer, dry conifer, mixed and deciduous). Among the three regrowth categories, the largest percentage increase in snow mapped occurred in the 'older regrowth', while the least increase occurred in the 'young regrowth'. It appears that the proposed algorithm changes tend to have the greatest effect at higher canopy densities. Only small differences exist in the two classifications on 'frozen lakes' and in 'disturbed areas', which is as expected.

The proposed modifications to the MODIS snow-cover mapping algorithm increase the total area mapped as snow and significantly lower the variability in area mapped as snow between the three winter scenes (Table IV). In the original classification, the percentage of snow mapped between the three winter scenes varied from 67.2 to 99.3%. In the revised algorithm, the range was decreased (86.6 to 99.9%). While it is possible that the variability observed in the results of the original algorithm is indeed real, caused by snow cover being less than the assumed 100%, this is doubtful for two reasons. The first is that observations made in the SSA during acquisition of the February 1995 TM scene show snow cover to be essentially 100%. Thus, deviations from the 100% assumption represent real errors of omission in both algorithms. The second is that, from extensive testing of the current algorithm, it is known that the largest problem is failure to detect

snow when it exists, not incorrectly mapping non-snow-covered pixels as containing snow. Thus, it is most likely that the greater number of pixels mapped by the algorithm revisions are the result of correctly identifying more pixels containing snow rather than incorrectly mapping pixels that do not contain snow as snow covered.

For the two summer scenes, only in the case of dry conifer forests does the modification increase commission errors (i.e. incorrectly mapping snow in the summer scenes). However, the increases in commission errors are quite low (less than 0.1%). Overall, the proposed changes to the MODIS snow-cover mapping algorithm significantly increase the area mapped as snow during the winter months in the BOREAS SSA. An example of both classifications for a portion of the 6 February Landsat TM scene is shown in Figure 11.

From these comparisons, the revised MODIS snow-mapping algorithm appears to do a better job than the current algorithm at mapping snow in the BOREAS SSA. We recognize that the TM comparisons are necessarily limited to the two simplest cases: totally snow covered and totally snow free. However, the lack of TM scenes and detailed ancillary information on snow cover extent for the transitional periods when snow cover extent lies between these extremes precludes comparing the algorithms under these conditions.

Based on the model results, several statements concerning the ability of the MODIS snow mapping algorithm to map snow in the transitional cases can be made. The early winter case, where snow tends to be found in the open spaces and not under the canopy, should pose few problems to either the current or revised algorithm. In forested areas, both algorithms appear to classify a pixel as snow, even if snow only occupies a small fraction of the pixel (Figure 10). The presence of unfrozen water appears to have little effect as well, so unless open water comprises a large percentage of a pixel, the pixel should be classified as containing snow.

The spring situation, where snow persists under the canopy longer than in the clearings as discussed by Pomeroy and Granger (1997), presents a more serious limitation. As is shown in Figure 9, neither algorithm maps snow under high amounts of canopy cover or where leaf litter comprises a significant portion of the background. Thus, it is likely that in spring, where snow resides mostly under the canopy, total snow cover extent may be underestimated. Thus the snow-mapping errors are likely to be larger during spring snowmelt than at other times during the year.

Despite limitations in our ability to compare the snow-mapping results of the two algorithms, it does appear that the proposed revisions will provide real improvements in the performance of the MODIS snow-mapping algorithm. These results do not constitute final validation of the proposed changes to the MODIS snow mapping algorithm. Currently, there are extensive ongoing efforts to compare the performance of the two algorithms in both forested and other biomes, the results of which will determine whether or not the proposed changes are implemented as part of the at-launch version of the MODIS snow-mapping algorithm.

CONCLUSIONS

Because forests comprise a large fraction of the seasonally snow-covered portions of the world, accurate mapping of snow in forests is important. Forests present special problems in mapping snow from spaceborne instruments, since the canopy obscures the snow cover beneath and causes considerable shading. However, snow-covered forests are spectrally distinct from snow-free forests. Minor changes to the current MODIS snow-mapping algorithm will enable more accurate classification of snow-covered forests without sacrificing the algorithm's simplicity and computational frugality.

Canopy models coupled with snow reflectance models provide a valuable tool for assessing the performance of the MODIS snow mapping algorithm. An extreme range of snow and canopy conditions, solar illumination angles and view geometries will be encountered in the global mapping of snow using MODIS. After launch, canopy models can help to assess the performance of the MODIS snow cover mapping algorithm under a wider range of conditions than can be measured in the field.

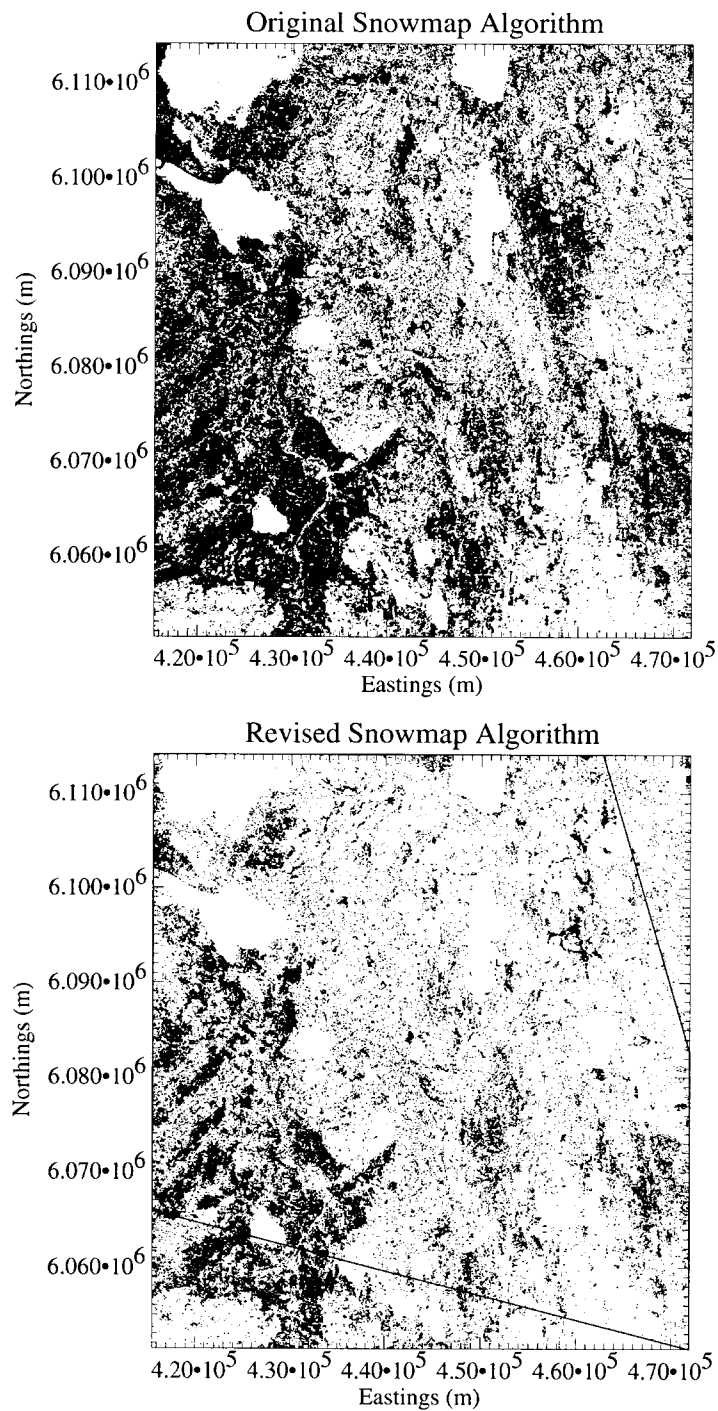


Figure 11. Comparison of original (top) and revised (bottom) MODIS snow cover mapping algorithms for a portion of the 6 February 1994 Landsat TM scene surrounding Prince Albert National Park. Snow-covered areas appear white

ACKNOWLEDGEMENTS

The authors wish to thank K. Fred Huemmrich (University of Maryland) for his assistance with the GeoSAIL modelling and Janet Chien (General Sciences Corporation) for computer support.

REFERENCES

- Ackerman, S., Strabala, L., Menzel, P., Frey, R., Moeller, C., Gumley, L., Baum, B., Schaff, C., Riggs, G., and Welch, R. 1996. 'Discriminating clear-sky from cloud with MODIS', *Algorithm Theoretical Basis Document (MOD35)*, Version 3-0, 109pp. available at <http://eosps0.gsfc.nasa.gov>
- Alexander, L. 1983. 'SAIL canopy model FORTRAN Software', *NASA Technical Report JSC-18899*.
- Bohren, C. F. and Barkstrom, B. R. 1974. 'Theory of the optical properties of snow', *J. Geophys. Res.*, **79**, 4527–4535.
- Bunting, J. T. and d'Entremont, R. P. 1982. 'Improved cloud detection utilizing defense meteorological satellite program near infrared measurements', *Environmental Research Paper No. 765*, AFGL-TR-82-0027. Air Force Geophysics Laboratory Hanscom AFB, MA.
- Carroll, T. R., Baglio, J. V., Verdin, J. P., and Holroyd, E. W., III. 1989. 'Operational mapping of snow cover in the United States and Canada using airborne and satellite data', *Proceedings of the 15th Canadian Symposium on Remote Sensing. V. 3. IGARSS'89, 10–14 July 1989, Vancouver, Canada*.
- Clark, R. N., Swayze, G. A., Gallagher, A. J., King, T. V. V., and Calvin, W. M. 1993. 'The U.S. Geological Survey, digital spectral library: Version 1: 0.2 to 3.0 microns', *US Geological Survey Open File Report, 93-592*. US Geological Survey, Denver, CO. 1340pp. A digital version of the newest library is available at <http://speclab.cr.usgs.gov/spectral.lib04/spectral-lib04.html>
- Dozier, J. 1989. 'Spectral signature of alpine snow cover from the Landsat Thematic Mapper', *Remote Sens. Environ.*, **28**, 9–22.
- Dozier, J., Davis, R. E., Chang, A. T. C., and Brown, K. 1988. 'The spectral bidirectional reflectance of snow', in *Spectral Signatures of Objects in Remote Sensing, Fourth International Colloquium, ESA SP-287, Paris*. pp. 87–92.
- Fily, M., Bourdelles, B., Dedieu, J. P., and Sergent, C. 1997. 'Comparison of *in situ* and Landsat Thematic Mapper derived snow grain characteristics in the Alps', *Remote Sens. Environ.*, **59**, 452–460.
- Foster, J. L. and Chang, A. T. C. 1993. 'Snow cover', in Gurney, R. L., Parkinson, C. L., and Foster, J. L. (eds), *Atlas of Satellite Observations Related to Global Change*. Cambridge University Press, Cambridge. pp. 361–370.
- Hall, D. K. 1988. 'Assessment of polar climatic change using satellite technology', *Rev. Geophys.*, **26**, 26–39.
- Hall, F. G., Huemmrich, K. F., Strelbel, D. E., Goetz, S. J., Nickeson, J. E., and Woods, K. D. 1992. 'Biophysical, morphological, canopy optical property and productivity data from the Superior National Forest', *NASA Technical Memorandum 104568*. NASA, Greenbelt, 137pp.
- Hall, D. K., Riggs, G. A., and Salomonson, V. V. 1995. 'Development of methods for mapping global snow cover using moderate resolution imaging spectroradiometer data', *Remote Sens. Environ.*, **54**, 127–140.
- Hall, D. K., Foster, J. L., Chang, A. T. C., Benson, C. S., and Chien, J. Y. L. in press. 'Determination of snow-covered area in different land covers in central Alaska from aircraft data—April 1995', *Ann. Glaciol.* 1998. v 26.
- Harding, R. J. and Pomeroy, R. J. 1996. 'The energy balance of the winter boreal landscape', *J. Climatol.*, **9**, 2778–2787.
- Huemmrich, K. F. 1995. An analysis of remote sensing of the fraction of absorbed photosynthetically active radiation in forest canopies. Ph.D. thesis University of Maryland. 207 pp.
- Jasinski, M. F. and Eagleson, P. S. 1989. 'The structure of red-infrared scattergrams of semivegetated landscapes', *IEEE Trans. Geosci. Remote Sens.*, **27**, 441–451.
- Jasinski, M. F. and Eagleson, P. S. 1990. 'Estimation of subpixel vegetation cover using red-infrared scattergrams', *IEEE Trans. Geosci. Remote Sens.*, **28**, 253–267.
- Kyle, H. L., Curran, R. J., Barnes, W. L., and Escoe, D. 1978. 'A cloud physics radiometer', in *Third Conference on Atmospheric Radiation*. American Meteorological Society, Davis. pp. 107–109.
- Li, X. and Strahler, A. H. 1986. 'Geometric-optical bidirectional reflectance modeling of a conifer forest canopy', *IEEE Trans. Geosci. Remote Sens.*, **24**, 906–919.
- Loveland, T. R. and Belward, A. S. 1997. 'The IGBP-DIS global 1 km land cover data set, DISCover: first results', *Int. J. Remote Sens.*, **18**, 3289–3295.
- Markham, B. L. and Barker, J. L. 1986. 'Landsat MSS and TM post-calibration dynamic ranges, exoatmospheric reflectances and at-satellite temperatures', *EOSAT Tech. Notes*, **1**, 3–8.
- Matson, M. 1991. 'NOAA satellite snow cover data', *Palaeogeog. Palaeoclimatol. Palaeoecol.*, **90**, 213–218.
- Matson, M., Roeplewski, C. F., and Varnadore, M. S. 1986. *An Atlas of Satellite Derived Northern Hemisphere Snow Cover Frequency*. National Weather Service, Washington, D.C. 75 pp.
- Meador, W. E. and Weaver, W. R. 1980. 'Two-stream approximations to radiative transfer in planetary atmospheres: a unified description of existing methods and a new improvement', *Journal of the Atmospheric Sciences*, **37**, 630–643.
- National Snow and Ice Data Center, 1996. *Northern Hemisphere EASE-Grid Weekly Snow Cover and Sea Ice Extent*. Volumes 1.0–2.0.
- O'Brien, H. W. and Munis, R. H. 1975. 'Red and near-infrared spectral reflectance of snow', in Rango, A. (ed.), *Operational Applications of Satellite Snowcover Observations*, NASA SP-391. NASA, Greenbelt. pp. 345–360.
- Pomeroy, J. W. and Dion, K. 1996. 'Winter radiation extinction and reflection in a boreal pine canopy: measurements and models', *Hydrol. Process.*, **10**, 1591–1608.
- Pomeroy, J. W. and Granger, R. J. 1997. 'Sustainability of the western Canadian boreal forest under changing hydrological conditions. I. Snow accumulation and ablation', in Rosbjerg, D., Nour-Eddine, B., Gustard, A., Kundzewicz, Z. K. and Rasmussen, P. F. (eds), *Sustainability of Water Resources under Increasing Uncertainty*, IAHS Publ. No. 240. IAHS Press, Wallingford. pp. 237–242.

- Riggs, G. A., Hall, D. K., and Salomonson, V. V. 1994. 'A snow index for the Landsat Thematic Mapper and Moderate Resolution Imaging Spectroradiometer', *Proceedings of the International Geoscience and Remote Sensing Symposium, IGARSS '94, 8–12 August 1994, Pasadena, California*, pp. 1942–1944.
- Robinson, D. A. and Kukla, G. 1985. 'Maximum surface albedo of seasonally snow covered lands in the Northern Hemisphere', *J. Climate Appl. Meteorol.*, **24**, 402–411.
- Robinson, D. A., Dewey, K. F., and Heim, R. R. 1993. 'Global snow cover monitoring: an update', *Bull. Am. Meteorol. Soc.*, **74**, 1689–1696.
- Rosenberg, N. J., Blad, B. L., and Verma, S. B. 1983. *Microclimate: The Biological Environment*, 2nd edn. John Wiley & Sons, Inc. New York. 495pp.
- Rosenthal, W. 1993. 'Mapping montane snow cover at subpixel resolution from the Landsat Thematic Mapper', *MA Thesis*, University of Calif., Santa Barbara.
- Rosenthal, W. and Dozier, J. 1996. 'Automated mapping of montane snow cover at subpixel resolution from the Landsat Thematic Mapper', *Wat. Resour. Res.*, **32**, 115–130.
- Salomonson, V. V., Toll, D. L., and Lawrence, W. T. 1992. 'Moderate resolution imaging spectroradiometer (MODIS) and observations of the land surface', in *International Geoscience and Remote Sensing Society Annual Meeting (IGARSS'92)*, Houston, Texas, pp. 549–551.
- Salisbury, J. W. and D'Aria, D. M. 1992. 'Emmissivity of terrestrial materials in the 8–14 μm atmospheric window', *Remote Sens. Environ.*, **42**, 83–106.
- Salisbury, J. W. and D'Aria, D. M. 1994. 'Emmissivity of terrestrial materials in the 3–5 μm atmospheric window', *Remote Sens. Environ.*, **47**, 345–361.
- Salisbury, J. W., D'Aria, D. M., and Wald, A. 1994. 'Measurements of the thermal infrared spectral reflectance of frost, snow, and ice', *J. Geophys. Res.*, **99**, 24, 235–24, 240. The John Hopkins spectral library can be accessed via: <http://asterweb.jpl.nasa.gov/speclib/>
- Sellers, P., Hall, F., Margolis, H., Kelly, B., Baldocchi, D., den Hartog, G., Chihlar, J., Ryan, M. G., Goodison, B., Crill, P., Ranson, K. J., Lettenmaier, D., and Wickland, D. E. 1995. 'The Boreal Ecosystem–Atmosphere Study (BOREAS): an overview and early results from the 1994 field year', *Bull. Am. Meteorol. Soc.*, **76**, 1549–1577.
- Verhoef, W. 1984. 'Light scattering by leaf layers with application to canopy reflectance modelling: the SAIL model', *Remote Sens. Environ.*, **16**, 125–141.
- Warren, S. G. 1982. 'Optical properties of snow', *Rev. Geophys. Space Phys.*, **20**, 67–89.
- Warren, S. G. and Wiscombe, W. J. 1980. 'A model for the spectral albedo of snow. II: snow containing atmospheric aerosols', *J. Atmos. Sci.*, **37**, 2734–2745.
- Wiscombe, W. J. and Warren, S. G. 1980. 'A model for the spectral albedo of snow: 1: pure snow', *J. Atmos. Sci.*, **37**, 2712–2733.
- Woodcock, C. E., Collins, J. B., Jakabhazy, V. D., Li, X., Macomber, S. A. and Y. Wu, Y. 1997. 'Inversion of the Li–Strahler canopy reflectance model for mapping forest structure', *IEEE Trans. Geosci. Remote Sens.*, **35**, 405–414.